

Investigation of light-induced drift of sodium vapor

S. N. Atutov, I. M. Ermolaev, and A. M. Shalagin

Institute of Automation and Electrometry, Siberian Division, USSR Academy of Sciences

(Submitted 4 August 1986)

Zh. Eksp. Teor. Fiz. **92**, 1215–1227 (April 1987)

Light-induced drift (LID) of sodium vapor in the inert buffer gases He, Ne, Ar, Kr, and Xe is investigated in the absence of physical adsorption. The elimination of physical adsorption provides new opportunities for a quantitative study of LID. The measured dependences of the sodium-vapor density on the coordinates and time agree well with the theoretical calculations. The experiment has yielded the diffusion coefficients of sodium in inert gases and the relative changes of the collision transport frequencies of excited sodium atoms.

1. INTRODUCTION

A new gaskinetic phenomenon in a radiation field, light-induced drift (LID), was predicted¹ and experimentally observed² in 1979 and has been actively investigated theoretically and experimentally ever since (see, e.g., Ref. 3 and the citations therein). Interest in this phenomenon is due mainly because it offers promise of scientific and practical applications, particularly for finding the transport properties of excited states of atoms and molecules, for separation of the components of gas mixtures (including isotopes, isomers, and others), for recording extremely low concentrations, and others.

In the first experiment² it was shown, with sodium vapor mixed with neon and helium gases as buffers, that the LID effect can manifest itself very strongly. No detailed investigation aimed at obtaining quantitative data and at comparison with experiment was carried out at that time. This was due to the extremely high chemical activity of the sodium vapor and to the masking effect of vapor adsorption by the glass-cell walls. Owing to their chemical activity, the sodium vapor did not advance far along the cell. The presence of physical adsorption, on the other hand, led to a very long (10–15 min) time to establish stationary distribution of the sodium-vapor concentration. The reason is that the physical adsorption of the sodium turned out to be much larger on the inner surface of the cell than in its volume. In the upshot, "wiping" the sodium off the surface or its "saturation" by the action of the LID were very slow processes.

The difficulty of overcoming the adsorption problem governed the further development of experimental research into LID,^{4,9} mainly as applied to objects (primarily molecular) for which this problem does not exist. On the other hand, theory¹⁰ predicted the strongest manifestations of LID in atomic objects optically excited from the ground state. For the available laser-radiation sources, these objects are the vapors of alkali metals and or alkaline-earth and rare-earth elements. It is for these substances that the effects of adsorption and chemical activity are strongest.

The authors of a relatively recent paper¹¹ (see also Ref. 12) were able to decrease somewhat the influence of sodium-vapor adsorption (apparently by using a special type of glass) and demonstrated clearly the LID effect in the optical-piston regime predicted in Ref. 10. In the experiments of Refs. 11 and 12, however, owing to the residual influence of physical adsorption, the piston speed was still lower by several orders than predicted by the theory.

One of us has found a final solution to the problem of physical adsorption.¹³ It was found that such a simple measure as coating the inner walls of the cell with a VM-1 oil film eliminates completely the physical adsorption of the sodium vapor. In the same experimental geometry as in Ref. 2, the time to establish a stationary distribution of the vapor density in the LID process was decreased from 10–15 min (Ref. 2) to several milliseconds,¹³ i.e., by five decades. As a result, a sodium-vapor velocity 580 cm/s in helium buffer gas was achieved in Ref. 13, and it was shown there that LID can be used to concentrate vapor in a cell region shorter than a millimeter.

The work reported in Ref. 13 has thus revealed the feasibility of a detailed quantitative study of LID of atoms. We report here the results of an experimental investigation of LID of sodium vapor in various buffer gases (He, Ne, Ar, Kr, Xe).

2. EXPERIMENTAL SETUP

The principal units of the experimental setup (Fig. 1), which is similar to that used in Refs. 2 and 13, were a dye laser 1 continuously tunable in frequency near the sodium D_1 and D_2 lines, and a cell 2 containing sodium vapor in a buffer gas. The laser radiation power reached 70 mW at an approximate spectral width 1 GHz. The distribution of the sodium-vapor density along the absorbing cell was made visible by the vapor fluorescence, and quantitative information was obtained with a movable photoreceiver 3 connected to an automatic plotter 4 or an oscilloscope 5. A photoreceiver 6 recorded the laser radiation power passing through the cell. The difference between the densities at two different points was measured with a differential photoreceiver 7 and a microammeter 8.

The cell was a glass capillary with inside diameter 1 mm and length 49 cm. Sodium vapor was admitted through a stub 9 and lateral orifice at the midpoint of the cell. The vapor admission rate was regulated by autonomous heating of the stub. The capillary temperature ranged from 20 to 85 °C. Connected to the ends of the cell were heated gas absorbers 10 with which the admitted buffer gas could be cleared of impurities (hydrogen, in particular). To admit and exhaust the buffer gases, the cell was connected to a vacuum post. The end faces of the cell were sealed with picein-glued windows.

Special pains were taken to rid the inner surface of the cell of traces of adsorbed water and active gases. This was

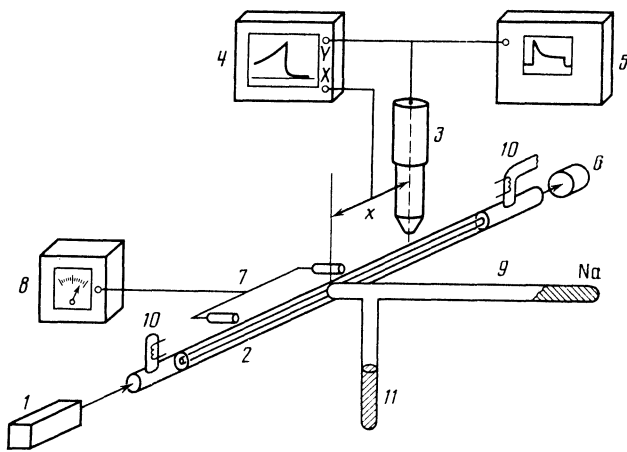


FIG. 1. Diagram of experimental setup (the callouts are in the text).

done with a dc glow discharge in neon at a current ≈ 30 mA (the role of gas absorbers was assumed here by the internal electrodes). The cell was regarded as ready for operation if a glow discharge in a fresh batch of neon did not change color in an hour.

After cleaning, the inner surface of the cell was "passivated." As a rule, paraffin was used for this purpose, since it was shown by special investigations, in which various brands of diffusion oil (VM-1, PFMS-2, 5F4É) and also paraffin and polyethylene were compared, the most inert to sodium vapor were the already used¹³ VM-2 oil and particularly paraffin. The remaining substances bind sodium vapor too strongly chemically and prevent it from advancing far along the capillary.

To coat its inner surface the cell was continuously pumped out, paraffin was heated in stub 11 and its vapor condensed on the inner surface of the cell and formed a film whose presence was readily monitored visually.

To prevent loss of radiation and glare formation by reflection from the inner walls of the capillary, the laser beam was guided along the capillary axis and focused with a lens in such a way that the diameter of the light beam in the capillary did not exceed 0.5 mm, or half the inside diameter of the capillary.

3. THEORY

Owing to fine and hyperfine splitting, the sodium atom has a complicated structure of the levels that interact with the laser radiation. Calculation of the LID effect in such a multilevel situation, with all the details taken into account, becomes very laborious. Fortunately, some circumstances allow the problem to be simplified during the first stages of the LID research, by highlighting the principal factors and permitting the fine details to be neglected.

The excited state of a sodium atom, with allowance for the fine and hyperfine splitting, and also for the level degeneracy, is represented by 24 sublevels. It is known, however, that collisions cause strong mixing of the sodium P -state sublevels, including also the fine-splitting components.¹⁴ In one collision act, with an impact parameter corresponding to large-angle scattering (these are precisely the collisions of importance in LID), the atom can encounter all the sublevels of the P state, so that the result of the collision is independent of the sublevel on which the atom was located prior to

the collision. In other words, there exist unified transport properties for the P -state as a whole (see also Ref. 15). Formally this means that the function $\rho_m(\mathbf{v})$ that represents the distribution of the total P -state population in velocity satisfies the kinetic equation.

$$(\partial/\partial t + \Gamma_m + \gamma + \mathbf{v}\nabla)\rho_m(\mathbf{v}) = S_m + Np(\mathbf{v}). \quad (1)$$

Here Γ_m is the radiative-decay constant, N the density of the sodium atoms, $p(\mathbf{v})$ the number of events, per unit time and per unit velocity interval, in which an atom absorbs radiation, γ a constant characterizing the loss of sodium by chemical bonding, and S_m the collision integral, which takes under the foregoing conditions the form

$$S_m = \int [A_m(\mathbf{v}|\mathbf{v}_1)\rho_m(\mathbf{v}_1) - A_m(\mathbf{v}_1|\mathbf{v})\rho_m(\mathbf{v})]d\mathbf{v}_1, \quad (2)$$

where $A_m(\mathbf{v}|\mathbf{v}_1)$ is the kernel of the collision integral.

Matters are somewhat more complicated with the ground state. The hyperfine splitting components, separated by frequency intervals 1772 MHz, are practically not mixed by the collisions¹⁶ and have therefore individual transport properties. There are no known data on the ratio of these properties at present. If they differ greatly, the dependence of the LID effects on the radiation frequency may become greatly distorted.¹⁵ Getting ahead of ourselves, we note that no noticeable distortion of this dependence was observed in our experiment, so that it can be stated that the transport properties of the hyperfine components of the ground state of sodium are approximately the same. If the differences between them are neglected it suffices, for the ground state, to consider the total-population velocity distribution $\rho_n(\mathbf{v})$, which satisfies the equation

$$(\partial/\partial t + \gamma + \mathbf{v}\nabla)\rho_n(\mathbf{v}) = S_n + \Gamma_m\rho_m(\mathbf{v}) - Np(\mathbf{v}), \quad (3)$$

where S_n satisfies Eq. (2) with m replaced by n .

Thus, from the standpoint of collisions with large-angle scattering, Eqs. (1) and (2) describe a certain effective two-level system. The presence of many levels is manifested only in the quantity $p(\mathbf{v})$, the evaluation of which calls, of course, for more detailed kinetic equations. It is not our aim here to determine $p(\mathbf{v})$, since many quantitative data can be obtained even without specifying $p(\mathbf{v})$.

We integrate now Eqs. (1) and (2) with respect to the velocities. The collision quenching and excitation of the P states are negligibly small, so that $\int S_i d\mathbf{v} = 0$, and we have

$$(\partial/\partial t + \Gamma_m + \gamma)N_m + \text{div } \mathbf{j}_m = Np, \quad p \equiv \int p(\mathbf{v})d\mathbf{v}, \quad (4)$$

$$(\partial/\partial t + \gamma)N_n + \text{div } \mathbf{j}_n = \Gamma_m N_m - Np, \quad \mathbf{j}_i \equiv \int \mathbf{v}\rho_i(\mathbf{v})d\mathbf{v}.$$

Here N_m and N_n are the populations integrated over the velocities, and \mathbf{j}_m and \mathbf{j}_n are the fluxes of the atoms in the states m and n . Equation (4) leads to the following obvious continuity equation

$$\partial N/\partial t + \gamma N + \text{div } \mathbf{j} = 0, \quad \mathbf{j} \equiv \mathbf{j}_m + \mathbf{j}_n. \quad (5)$$

In the first equation of (4) we can neglect the derivatives with respect to time and coordinate, since the characteristic time scale of N_m is substantially larger than $\Gamma_m^{-1} \sim 10^{-8}$ s, and the spatial scale of variation of \mathbf{j}_m is larger than $\bar{v}/\Gamma_m \sim 10^{-3}$ cm. In this case we obtain in lieu of (4)

$$N_m = Np / (\Gamma_m + \gamma), \quad (6)$$

which together with (5) is the equivalent of Eq. 4.

We now obtain equations for the fluxes \mathbf{j}_m and \mathbf{j}_n . We note first, however, that

$$\int S_i \mathbf{v} d\mathbf{v} = - \int v_i^{tr}(\mathbf{v}) v \rho_i(\mathbf{v}) d\mathbf{v} = -v_i \mathbf{j}_i, \\ v_i^{tr}(\mathbf{v}) = \int \left(1 - \frac{\mathbf{v}\mathbf{v}_1}{v^2} \right) A_i(\mathbf{v}_1 | \mathbf{v}) d\mathbf{v}_1, \quad (7)$$

where $v_i^{tr}(\mathbf{v})$ is the so-called transport frequency of the collisions (see, e.g., Refs. 17 and 18 for its connection with the transport cross section), which depends in general on the velocity. The coefficient v_i in (7) depends therefore on the actual form of the disequilibrium of the velocity distribution, i.e., in final analysis, on the characteristics (frequency, intensity, and others) of the radiation. As shown in Ref. 18, however, in the overwhelming majority of cases this dependence can be neglected, and the coefficients v_i (the averaged transport frequencies of the collisions) can be regarded as purely collisional properties.

We multiply Eqs. (1) and (3) by \mathbf{v} and integrate over the velocities. Taking (7) into account, we obtain (we neglect γ , since actually $\gamma \lesssim 10^2 \text{ s}^{-1}$ and is significant only in the continuity equation (5))

$$(\partial/\partial t + \Gamma_m + \nu_m) \mathbf{j}_m + (\bar{v}^2/2) \nabla N_m = N(k/k) \bar{v} Q, \quad \bar{v} = (2k_B T/M)^{1/2},$$

$$(\partial/\partial t + \nu_n) \mathbf{j} + (\bar{v}^2/2) \nabla N = (\nu_n - \nu_m) \mathbf{j}_m, \quad (8) \\ Q = \int (\mathbf{k}\mathbf{v}/k\bar{v}) p(\mathbf{v}) d\mathbf{v}.$$

Here M is the atom mass, T the temperature, and k_B Boltzmann's constant. The terms ∇N_m and ∇N in (8) were obtained under the assumption that the atom distribution in velocity differs on the whole little from Maxwellian. In addition, it was recognized that $p(\mathbf{v})$ is asymmetric in a direction collinear with the radiation wave vector \mathbf{k} .

The external conditions vary slowly in the scale of $(\Gamma_m + \nu_m)^{-1}$, so that the derivative with respect to time can certainly be neglected in the first equation of (8). Substituting \mathbf{j}_m of the first equation in the second and taking (6) into account, we obtain the following equation for the flux \mathbf{j} :

$$\left(\frac{\partial}{\partial t} + \nu_n \right) \mathbf{j} = - \frac{\bar{v}^2}{2} \nabla \left[N \left(1 + \frac{\nu_n - \nu_m}{\Gamma_m + \nu_m} \frac{p}{\Gamma_m} \right) \right] \\ + \frac{\nu_n - \nu_m}{\Gamma_m + \nu_m} N \bar{v} \frac{\mathbf{k}}{k} Q. \quad (9)$$

In this equation it is easy to discern the onset of an atom flux, both on account of the LID effect, for which the term proportional to Q is responsible, and on account of the light-induced diffusion pulling (expulsion) into a region of higher radiation intensity¹⁹ (an effect due to the coordinate dependence of p). Both effects are proportional to the difference $\nu_n - \nu_m$ of the collision transport equations.

If the buffer-gas pressure is such that the mean free path (\bar{v}/ν_n) is much smaller than the cell diameter, the principal flux relaxation channel is via collisions with the buffer gas. The characteristic time ν_n^{-1} is significantly shorter than the time of variation of the macroscopic conditions, so that the derivative with respect to time in (9) can be neglected, and hence

$$\mathbf{j} = -\nabla(DN) + \mathbf{u}N, \quad (10)$$

$$D = \frac{\bar{v}^2}{2\nu_n} \left(1 + \frac{\nu_n - \nu_m}{\Gamma_m + \nu_m} \frac{p}{\Gamma_m} \right), \quad \mathbf{u} = \bar{v} \frac{\nu_n - \nu_m}{\nu_n} \frac{Q}{\Gamma_m + \nu_m} \frac{\mathbf{k}}{k}.$$

The quantity D has the meaning of an effective diffusion coefficient, and \mathbf{u} is the velocity of the light-induced drift.

Substitution of (10) in the continuity equation (5) yields an equation for the atom density:

$$\partial N/\partial t + \text{div}(\mathbf{u}N - \nabla DN) + \gamma N = 0. \quad (11)$$

At $\nu_n = \nu_m$ and $\gamma = 0$ this equation leads to the usual diffusion equation.

Under the conditions of our experiments (long capillary) Eq. (11) can be reduced to one-dimensional. The density in the capillary cross section is practically uniform. To take a possible residual influence of physical adsorption into account, we proceed as follows. We characterize the adsorption by the time τ_a spent by the atoms on the surface. Under equilibrium conditions the surface density n_σ is connected with the bulk density by the relation $n_\sigma = \bar{v}N\tau_a/4$. Assume that in the LID process or in diffusion the balance between the bulk and surface densities is not disturbed; the one-dimensional equivalent of (11) is then

$$\frac{\partial N_{\text{eff}}}{\partial t} + \frac{\partial}{\partial x} \left(\mathbf{u}N - \frac{\partial}{\partial x} DN \right) + \gamma N = 0, \quad N_{\text{eff}} = N \left(1 + \frac{\bar{v}\tau_a}{2r} \right), \quad (12)$$

where r is the radius of the capillary. (A similar equation, but for $\gamma = 0$, was used in Ref. 20 in an analysis of an optical piston.) Note that the drift velocity u and the diffusion coefficient D in this equation are averages of these characteristics over the cross section. We can make in (12) the substitution

$$\partial N_{\text{eff}}/\partial t \rightarrow \partial N/\partial t_{\text{eff}} \quad \text{where } t_{\text{eff}} = t(1 + \bar{v}\tau_a/2r)^{-1},$$

meaning a change in the time scale. Thus, in the presence of adsorption the process proceeds in the same manner, but more slowly than in its absence. We see that the adsorption does not affect the stationary distribution of the density (at a given value of γ).

We solve now the one-dimensional problem in a geometry that accords with the experiment, i.e., assuming that a source of sodium vapor operates at the center of the capillary ($x = 0$). The medium is assumed to be optically thin, so that u and D are independent of x . The stationary solution of (12) is obtained in elementary fashion:

$$N(x) = \begin{cases} N_0 \exp(-x/l_1), & x > 0, \\ N_0 \exp(x/l_2), & x < 0, \end{cases} \\ l_{1,2} = \left[\left(\frac{u^2}{4D^2} + \frac{\gamma}{D} \right)^{1/2} \mp \frac{u}{2D} \right]^{-1}. \quad (13)$$

In this simple case we obtain an exponential dependence of the density on the coordinate, and with different arguments of the exponential for $x > 0$ and $x < 0$ (the asymmetry due to the light-induced drift). In the absence of LID ($u = 0$) we have

$$N(x) = N_0 \exp(-|x|/l_0), \quad l_0 = (D/\gamma)^{1/2}. \quad (14)$$

The connection between the quantities l_1 , l_2 and l_0 is

$$l_0 = (l_1 l_2)^{1/2}. \quad (15)$$

In addition, one more relation is useful

$$(l_1 - l_2)/l_1 l_2 = u/D. \quad (16)$$

If the diffusion coefficient is known, we can obtain on the basis of (16) the drift velocity by measuring l_1 and l_2 . If l_1 and l_2 differ greatly (e.g., $l_1 \gg l_2$), we get $l_2 = D/u$, and to find u/D it suffices to measure only l_2 , which is the smallest of the characteristic dimensions.

We solve the nonstationary problem in the following formulation. A constant density N_0 is maintained at the point $x = 0$. The radiation is turned on to the instant $t = 0$. The initial condition is thus the distribution (14) and the boundary conditions are zero (owing to the chemical bonding). In the region $x > 0$ the solution $N(x, t)$ takes the form

$$\begin{aligned} N(x, t) = & \frac{N_0}{2} \left\{ \exp\left(\frac{x}{l_2}\right) \operatorname{erfc}\left[\frac{x}{2(Dt)^{1/2}} + \frac{(Dt)^{1/2}}{2} \left(\frac{1}{l_1} + \frac{1}{l_2}\right)\right] \right. \\ & + \exp\left(-\frac{x}{l_1}\right) \operatorname{erfc}\left[\frac{x}{2(Dt)^{1/2}} - \frac{(Dt)^{1/2}}{2} \left(\frac{1}{l_1} + \frac{1}{l_2}\right)\right] \\ & - \exp\left(-\frac{x+ut}{l_0}\right) \operatorname{erfc}\left[\frac{x}{2(Dt)^{1/2}} + \frac{(Dt)^{1/2}}{2} \left(\frac{1}{l_2} - \frac{1}{l_1} - \frac{2}{l_0}\right)\right] \\ & - \exp\left(\frac{x-ut}{l_0} + \frac{x}{l_1} - \frac{x}{l_2}\right) \\ & \times \operatorname{erfc}\left[\frac{x}{2(Dt)^{1/2}} - \frac{(Dt)^{1/2}}{2} \left(\frac{1}{l_2} - \frac{1}{l_1} - \frac{2}{l_0}\right)\right] \left. \right\} \\ & + N_0 \exp\left(-\frac{x+ut}{l_0}\right), \quad \operatorname{erfc}(z) \equiv 1 - \frac{2}{\pi^{1/2}} \int_0^z \exp(-\xi^2) d\xi. \end{aligned} \quad (17)$$

The solution for $x < 0$ is obtained from (17) by making the formal substitutions $u \rightarrow -u$ and $x \rightarrow |x|$.

If $u < 0$ and $l_1 \ll l_0 \ll l_2$, the solution of (17) in the region $x > l_1$ takes the simpler form

$$N(x, t) = N_0 \exp[-(x+ut)/l_0]. \quad (18)$$

In this case the density decreases exponentially with time, with a characteristic scale

$$\tau = l_0/u, \quad (19)$$

which does not depend on the coordinate x .

If the LID effect is small for some reason (low radiation intensity, proximity of its frequency to exact resonance, low buffer-gas pressure, etc.), then l_1 , l_2 , and l_0 are close to one another, and the relative change of the density is small. We can then obtain from (17)

$$\begin{aligned} \eta(x, t) \equiv \frac{\Delta N(x, t)}{\Delta N(x, 0)} = & \frac{(Dt)^{1/2}}{x} \left\{ 2 \left[\frac{x}{2(Dt)^{1/2}} - \frac{(Dt)^{1/2}}{l_0} \right] \right. \\ & + \exp\left(\frac{2x}{l_0}\right) \left[\frac{x}{2(Dt)^{1/2}} + \frac{(Dt)^{1/2}}{l_0} \right] \operatorname{erfc}\left[\frac{x}{2(Dt)^{1/2}} + \frac{(Dt)^{1/2}}{l_0}\right] \\ & - \left[\frac{x}{2(Dt)^{1/2}} - \frac{(Dt)^{1/2}}{l_0} \right] \operatorname{erfc}\left[\frac{x}{2(Dt)^{1/2}} - \frac{(Dt)^{1/2}}{l_0}\right] \left. \right\}, \\ \Delta N(x, t) = & N(x, t) - N(x, \infty). \end{aligned} \quad (20)$$

This expression does not contain the drift rate at all. This means that only the amplitude of the density variation depends on u , and the spatio-temporal behavior is determined entirely by the diffusion coefficient and by the independently

measured quantity l_0 . Thus, the conditions under which Eq. (20) is valid are favorable for finding the diffusion coefficient. In particular, if we track the density at the point $x = l_0$, then when the instant of time

$$t = l_0^2/2D = 1/2\gamma \quad (21)$$

is reached we have

$$\eta(l_0, t) = e^2 \operatorname{erfc}(\sqrt{\gamma}) \approx 0.34. \quad (22)$$

Consequently, the time in which $\eta(l_0, t)$ decreases to the level 0.34 is connected with l_0 and D by relation (21).

Of particular interest is the region of extremely low buffer-gas pressures, when the mean free path is much larger than the capillary diameter ($\nu_m, \nu_n \ll \bar{v}/2r \sim 10^6 \text{ s}^{-1}$), i.e., in the Knudsen regime. The conditions $\nu_m, \nu_n \ll \Gamma_m$ are then also satisfied with a large margin. If there is no buffer gas at all, there are obviously also no LID effects, so that the sodium-vapor density distribution remains symmetric about the point $x = 0$ in the discussed experimental setup. A small amount of buffer gas within the limits of the Knudsen conditions leads to an antisymmetric increment proportional to the buffer-gas pressure (actually, to the difference $\nu_m - \nu_n \equiv \Delta\nu$ between the transport frequencies of the collisions). Since the collision frequency is small compared with the radiation-relaxation constant, the absorption probability is insensitive to a small amount of buffer gas. Nor does the buffer gas influence the vapor diffusion along the capillary; under Knudsen conditions the momentum relaxation takes place on the walls. Thus, the buffer gas manifests itself in the LID effect at low pressure only via the factor $\Delta\nu$. This circumstance turns out to be very useful. Namely, by measuring the ratios of the LID effects for different types of buffer gas and constant radiation characteristics, we obtain by the same token the ratios of the values of $\Delta\nu$, i.e., the ratios of the differences of the transport characteristics for combining states.

4. EXPERIMENTAL RESULTS AND THEIR DISCUSSION

In its visual manifestation, the observed LID effect is a rather brilliant spectacle. As the radiation frequency is varied, one observes in the vicinity of the absorption-line center a glow on one half of the capillary, alternating with a glow on the other half. This is fluorescence of the sodium vapor that enters the capillary through the orifice at its midpoint. Under the conditions of the experiment, the fluorescence intensity is proportional to the sodium-vapor density. The glow is seen to "jump over" from one half of the capillary to the other almost instantaneously as it follows the rapid passage of the radiation frequency through resonance.

Both the stationary distribution of the sodium-vapor density and the changes of the density with time were measured. The stationary distribution was recorded at different values of the detuning Ω of the radiation frequency from the absorption-line center, at different radiation power, and at different pressures of the buffer gases He, Ne, Ar, Kr, and Xe. The variation of the density with time was recorded at different distances from the lateral orifice in the capillary. The differential photoreceiver was used whenever the LID was small. All the experiments were made at a capillary temperature 85 °C.

The LID effect is qualitatively the same for radiation

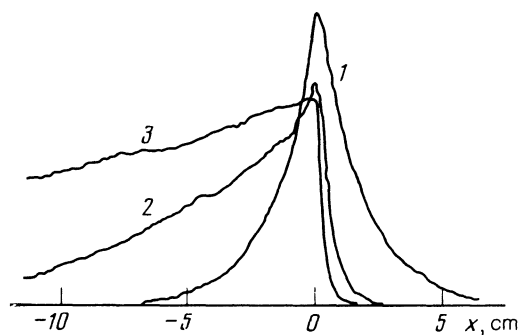


FIG. 2. Stationary distribution of the sodium-vapor density. The radiation propagates from left to right. 1 - $\Omega = 0$ (Ne); 2 - $\Omega \approx k\bar{v}$ (Ne); 3 - $\Omega \approx k\bar{v}$ (He).

frequency in the vicinity of either the D_1 or the D_2 line. All the quantitative results that follow are for excitation of the D_2 line.

Examples of the spatial distribution of the sodium-vapor density along the capillary at different values of Ω are shown in Fig. 2 (radiation power ≈ 50 mW, He or Ne pressure ≈ 10 Torr). It is seen from the figure that at $\Omega = 0$ the density distribution is symmetric about the lateral orifice ($x = 0$) and the chemical bonding of the sodium causes the density to decrease with distance from the cell center. At $\Omega \neq 0$ the distribution is strongly asymmetric. Reversal of the sign of Ω leads to inversion of curves 2 and 3 relative to the point $x = 0$. With allowance for the instrumental function of the photoreceiver, it can be stated that in the case of He at $\Omega \neq 0$ the sodium vapor advances less than 1 mm in the direction of $x > 0$.

The theoretical model contains an exponential loss of sodium by chemical bonding. To check this dependence we recorded the distribution of the sodium-vapor density $N(x)$ at $\Omega = 0$ and a low ($\lesssim 1$ mW) radiation power. In the entire investigated pressure range the loss was indeed exponential to within not more than several percent. The measured dependence of the exponent l_0 on the buffer-gas pressure (see Fig. 3 with helium as the example) leads to the conclusion that a chemical reaction takes place on the surface or in the volume. In the former case $\gamma \propto D$, so that $l_0 = (D/\gamma)^{1/2}$ should be independent of pressure. In the case of a volume chemical reaction with an active impurity of constant density we have $l_0 \propto P^{-1/2}$ (P is the buffer-gas pressure). This is precisely the dependence observed in the experiment. The sodium vapor reacts therefore chemically in the volume with a chemically active impurity (which, unfortunately, has not yet been identified); this impurity does not enter with the buffer gas, but is produced in the cell itself.

With the value $\Omega = 0$ maintained and the radiation power varied, we tracked the influence of the power on the effective diffusion coefficient. The variation of the latter at the maximum did not exceed 10%, so that the diffusion coef-

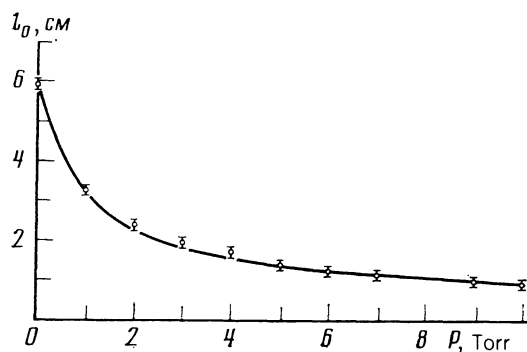


FIG. 3. Dependence of l_0 on the helium pressure.

ficient in (12) can be regarded as independent of the radiation power and as equal, at higher pressures, to the diffusion coefficient D_n of the unexcited sodium atom. The low sensitivity of D to the radiation power is due mainly to the small ratio of the light beam and capillary cross section areas.

The set of $N(x)$ curves of the type shown in Fig. 2, obtained in a wide range of the radiation parameters, pressures, and types of buffer gas, was reduced to check on Eq. (13) and to determine the parameters l_0 , l_1 , and l_2 . Reliable measurement results were obtained in the range of these parameters from 1 mm to 20 cm. The limits of this range are imposed by the construction (length and inside diameter) of the absorbing cell and by the spatial resolution of the photoreceiver. In all cases, the exponential law (13) held with accuracy not worse than 10%. Relation (15) was found to be valid with the same accuracy.

As indicated in the preceding section, if the diffusion coefficient D is known, the drift velocity can be obtained on the basis of l_1 and l_2 [see Eq. (16)]. The diffusion coefficient was obtained from time measurements combined with measurements of l_0 . The time measurements were carried out at a radiation power of several mW to ensure smallness of the LID. The laser radiation was interrupted with a chopper, and the variation of the density with time was recorded by photoreceiver 3 and oscilloscope 5, see Fig. 1. The results were reduced using Eqs. (21) and (22) assuming $t_{\text{eff}} = t$ [see (12) and below]. The diffusion coefficients were obtained by using the value of l_0 measured at the same time. The pertinent results are summarized in Table I (in which the only bulk diffusion coefficients are given, since these are of greatest interest). Corrected for the temperature dependence, or values of D for He, Ne, and Ar agree well with the published data²¹ and with our measurements based on the effective light-induced diffusive pulling (expulsion) of the particles into the light beam.²² As to the coefficients of sodium diffusion into Kr and Xe, they have apparently been obtained here for the first time.

TABLE I.

Buffer gas	D , cm ² /s (85 °C, 760 Torr)	D , cm ² /s (760 Torr)	D , cm ² /s (Ref. 23) (110 °C, 760 Torr)
He	0.70±0.06	0.65±0.09 [21], 85 °C	0.70±0.15
Ne	0.47±0.05	0.49±0.04 [22], 115 °C	0.35±0.06
Ar	0.28±0.03	0.27±0.20 [21], 85 °C	0.27±0.06
Kr	0.21±0.02	—	—
Xe	0.16±0.02	—	—

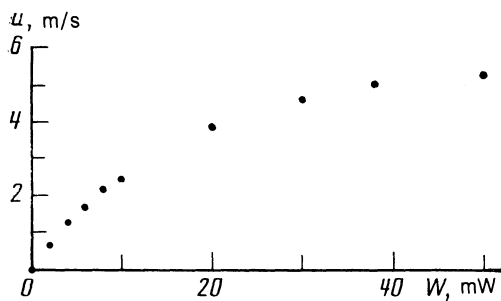


FIG. 4. Drift rate vs radiation power for Xe buffer gas at $P = 10$ Torr.

Since our results agree with those known for $t_{\text{eff}} = t$, this attests to a negligibly small influence of physical adsorption. This conclusion was additionally confirmed by comparison of the measured temporal and spatial drift velocities, performed under identical conditions $l_1 \ll l_0 \ll l_2$ [see (18)]. The temporal measurements were reduced using Eq. (18) and the obtained value of D . These results agreed within not more than 10%. It was thus proved that in our experiments there was practically no absorption of sodium vapor on the cell walls.

The most reliable (with lower systematic error) drift rate is determined from the data on l_1 and l_2 ; this method was therefore used for the most part. Plots of the drift velocity vs radiation power and vs pressure for the different buffer gases are similar. Examples are the dependence of u on the power for Xe as the buffer gas (Fig. 4) and on the pressure for He (Fig. 5), which were plotted in greatest detail. The radiation frequency in each experiment was chosen to maximize the LID effect.

The plot of Fig. 4 is initially linear in the radiation power, but tends subsequently to saturation. This behavior of the plot is in full agreement with the theoretical premises of the effect. The cause of the saturation is the velocity-selectivity decrease due to the field broadening of the absorption line. Still further increase of the intensity should decrease u , but such a power level has not yet been reached in experiment. The maximum of u is ≈ 6 m/s. It must be remembered, however, that the experimentally measured value of u is an average over the cross section of the capillary. The drift velocity on the light-beam axis is three to four times larger, since the beam cross section is smaller than that of the capillary by the same factor.

Three regions are clearly distinguishable on the plot of u vs helium pressure (Fig. 5). In the first region (0–0.7 Torr) the plot rises linearly with pressure, in the second (0.9–4 Torr) the drift velocity is almost constant, and in the third (> 4 Torr) it drops monotonically approximately in proportion to P^{-1} . The decrease of u towards higher pressures is easily explained by expression (10) for u . At $\nu_m > \Gamma_m$ the factor $1/(\Gamma_m + \nu_m)$ becomes proportional to

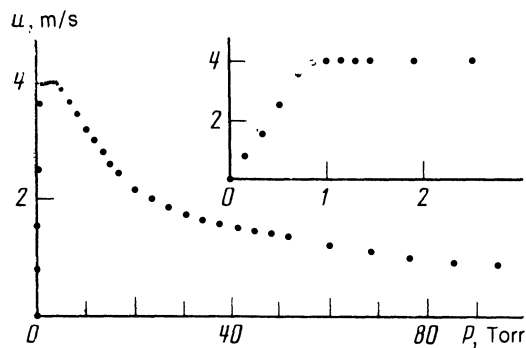


FIG. 5. Drift rate vs helium pressure. Radiation power 50 mW.

P^{-1} , and the factor Q can cause in principle further decrease. As the pressure is lowered, Eq. (10) for u yields a constant value; Q also becomes independent of pressure at $\nu_m \ll \Gamma_m$. This explains the middle section of the plot in Fig. 5. The experimental plot has in addition a region (at low pressures) where u is proportional to the pressure. This region is due to the geometry of the experiment: the mean free path in it exceeds the capillary diameter, and the diffusion coefficient is determined by collisions with the wall. This means formally that for the denominator of the factor $(\nu_n - \nu_m)/\nu_n$ in (10) one must replace ν_n by the frequency of the collisions with the wall. At low pressures this frequency is independent of pressure, and therefore $u \propto P$ here.

We consider finally the measurement of the difference $\Delta\nu = \nu_m - \nu_n$ of the transport frequencies of the collisions in the combining states of the sodium atom. The experimental procedure was the following. The buffer gas was first pumped out of the cell. The differential photoreceiver was mounted symmetrically with respect to the central orifice to make the difference signal (proportional to the density drop due to the action of the radiation) equal to zero. The signal remained equal to zero when the radiation frequency was changed, convincingly demonstrating the absence of the LID effect in the absence of the buffer gas. After this check, buffer gas was admitted through a batching valve. The pressure was chosen to be small enough to make the density drop (at the detuning Ω optimal for the LID) much less than the density itself. The Knudsen conditions were thereby automatically met. The buffer gas was changed without changing the radiation parameter.

As noted at the end of the preceding section, under Knudsen conditions the density drop is proportional to the difference and is dependent on the pressure only via this factor. Linearity in pressure was thoroughly verified for all the investigated buffer gases (He, Ne, Ar, Kr, Xe). The ratios of the curve slopes that are proportional to $\Delta\nu$ are gathered in Table II.

From the aggregate of the data on $\Delta\nu$ and on the diffusion coefficients it is possible to derive useful relations be-

TABLE II.

Buffer gas	$\Delta\nu/\Delta\nu_{\text{He}}$	$\frac{\Delta\nu/\nu_n}{(\Delta\nu/\nu_n)_{\text{He}}}$	$\Delta\nu/\nu_n$	$\Delta\nu/\nu_n$ [23]
He	1	1	0.14 ± 0.02	0.14 ± 0.02
Ne	0.39 ± 0.01	0.26 ± 0.03	0.037 ± 0.005	0.03 ± 0.005
Ar	5.2 ± 0.15	2.1 ± 0.2	0.29 ± 0.05	0.29 ± 0.02
Kr	8.2 ± 0.25	2.6 ± 0.3	0.37 ± 0.06	—
Xe	11.5 ± 0.35	2.6 ± 0.3	0.37 ± 0.06	—

tween the parameters $\Delta\nu/\nu_n$ for various buffer gases. These results are also given in Table II. The parameter $\Delta\nu/\nu_n$ for each separate gas is not determined accurately enough under the conditions of our experiment. This is due to systematic errors brought about by inaccurate knowledge of the radiation intensity inside the capillary and of the spectral composition of the radiation, which yields in the upshot only the parameter Q . The parameter $\Delta\nu/\nu_n$ is measured at present most accurately and reliably by using light-induced diffuse drawing-in (expulsion) effect, where the properties noted above (as well as many others) introduce no systematic errors. In particular, the parameter $\Delta\nu/\nu_n$ was measured quite accurately in Ref. 23 for sodium in a helium buffer. Knowing this result and the relations obtained in the present paper between the values of $\Delta\nu/\nu_n$ for different buffer gases, we can obtain the parameter $\Delta\nu/\nu_n$ for each individual buffer gas, as is demonstrated in Table II. The table lists also the values of $\Delta\nu/\nu_n$ obtained for Ne and Ar in Ref. 23.

The parameter $\Delta\nu/\nu_n$, which is the fundamental property of the LID effect, behaves irregularly as the buffer-gas particle mass is increased. On the whole, this parameter increases from He to Xe, but neon drops out of this sequence, and has much smaller $\Delta\nu/\nu_n$ than helium.

The parameter $\Delta\nu/\nu_n$ was determined by the method described above also by tuning the radiation frequency to the D_1 line. The results agree within the error limits with those of Table II. This is convincing evidence of the validity of the employed two-level model.

5. CONCLUSION

Elimination of the masking influence of physical adsorption offers great promise for quantitative investigation of the LID effect. This is quite convincingly demonstrated by the results of the present paper. Above all, the effect has become much more strongly manifested. The experimentally obtained relations agree well with the main conclusions of LID theory. Such important properties of LID as the characteristic antisymmetric dependence on the frequency detuning, and the vanishing of the effect when the radiation power is decreased and when the buffer gas is removed, clearly confirmed by experiment. The procedure developed permits simple and reliable measurement of the diffusion

coefficients of the absorbed particles in the ground state, and measurement of their changes due to optical excitation.

The authors are grateful to S. G. Rautian for interest in the work and for many valuable remarks, and also to F. Kh. Gel'mukhanov, S. P. Pod'yachev, and D. A. Shapiro for help with the experiment and for a discussion of the results.

¹F. Kh. Gel'mukhanov and A. M. Shalagin, *Pis'ma Zh. Eksp. Teor. Fiz.* **29**, 773 (1979) [*JETP Lett.* **29** 711 (1979)].

²V. D. Antsygin, S. N. Atutov, F. Kh. Gel'mukhanov, *et al.*, *ibid.* **30**, 262 (1979) [**30**, 243 (1979)].

³F. Kh. Gel'mukhanov, *Avtometriya*, No. 1 49 (1985).

⁴S. N. Atutov, P. L. Chapovsky, and A. M. Shalagin, *Opt. Commun.* **43**, 285 (1982).

⁵V. N. Panfilov, V. P. Strunin, and P. L. Chapovskii, *Zh. Eksp. Teor. Fiz.* **85**, 881 (1983) [*Sov. Phys. JETP* **58**, 510 (1983)].

⁶A. K. Folin and P. L. Chapovskii, *Pis'ma Zh. Eksp. Teor. Fiz.* **38**, 452 (1983) [*JETP Lett.* **38** 549 (1983)].

⁷L. I. Krasnoperov, V. N. Panfilov, V. P. Strunin, and P. L. Chapovskii, *ibid.* **39** 122 (1984) [**39**, 143 (1984)].

⁸P. L. Chapovskii and A. M. Shalagin, *Quant. Electron. (Moscow)* **12**, 2275 (1985) [*Sov. J. Quant. Electron.* **15**, 1500 (1985)].

⁹A. E. Bakarev, L. P. Makas', and P. L. Chapovskii, *ibid.* **13**, 30 (1986) [**16**, 16 (1986)].

¹⁰F. Kh. Gel'mukhanov and A. M. Shalagin, *Zh. Eksp. Teor. Fiz.* **78**, 1674 (1980) [*Sov. Phys. JETP* **51**, 839 (1980)].

¹¹H. G. C. Werij, J. P. Woerdman, J. J. M. Beenakker, and I. Kuscer, *Phys. Rev. Lett.* **52**, 2237 (1984)].

¹²H. G. C. Werij, J. E. M. Havaerkort, and J. P. Woerdman, *Phys. Rev. A* **33**, 3270 (1986).

¹³S. P. Atutov, Preprint No. 288, Inst. of Automation and Electrometry, Siberian Div., USSR Acad. Sci., 1984.

¹⁴E. L. Lewis, *Phys. Rep.* **58**, 1 (1980).

¹⁵A. I. Parkhomenko and A. M. Shalagin, Preprint No. 225, Inst. of Automation and Electrometry, Sib. Div. USSR Acad. Sci., 1984.

¹⁶W. Happer, *Rev. Mod. Phys.* **44**, 169 (1972).

¹⁷A. M. Shalagin, Abstract of doctoral dissertation, Novosibirsk, Inst. of Automation and Electrometry, Sib. Div. USSR Acad. Sci., 1982.

¹⁸F. Kh. Gel'mukhanov, L. V. Il'ichev, and A. M. Shalagin, Preprint No. 286, Inst. Automation and Electrometry, Sib. Div. USSR Acad. Sci., 1985.

¹⁹F. Kh. Gel'mukhanov and A. M. Shalagin, *Zh. Eksp. Teor. Fiz.* **77**, 461 (1979) [*Sov. Phys. JETP* **50**, 234 (1979)].

²⁰B. Nienhuis, *Phys. Rev. A* **31**, 1636 (1985).

²¹J. A. Silver, *J. Chem. Phys.* **81**, 5125 (1984).

²²F. A. Franz and A. Sieradzan, *Phys. Rev. A* **29**, 1569 (1984).

²³S. N. Atutov, S. P. Pod'yachev, and A. M. Shalagin, *Zh. Eksp. Teor. Fiz.* **91**, 416 (1986) [*Sov. Phys. JETP* **64**, 244 (1986)].

Translated by J. G. Adashko